



HAL
open science

Finite-temperature properties of the relaxor $\text{PbMg}_{1/3}\text{Nb}_{2/3}\text{O}_3$ from atomistic simulations

A Al-Barakaty, Sergey Prosandeev, Dawei Wang, B Dkhil, L Bellaiche

► **To cite this version:**

A Al-Barakaty, Sergey Prosandeev, Dawei Wang, B Dkhil, L Bellaiche. Finite-temperature properties of the relaxor $\text{PbMg}_{1/3}\text{Nb}_{2/3}\text{O}_3$ from atomistic simulations. *Physical Review B: Condensed Matter and Materials Physics (1998-2015)*, 2015, 91, pp.214117. 10.1103/PhysRevB.91.214117 . hal-01260145

HAL Id: hal-01260145

<https://hal.science/hal-01260145v1>

Submitted on 27 Aug 2020

HAL is a multi-disciplinary open access archive for the deposit and dissemination of scientific research documents, whether they are published or not. The documents may come from teaching and research institutions in France or abroad, or from public or private research centers.

L'archive ouverte pluridisciplinaire **HAL**, est destinée au dépôt et à la diffusion de documents scientifiques de niveau recherche, publiés ou non, émanant des établissements d'enseignement et de recherche français ou étrangers, des laboratoires publics ou privés.

Finite-temperature and key ingredients for relaxor properties of $\text{PbMg}_{1/3}\text{Nb}_{2/3}\text{O}_3$ revealed by atomistic simulations

A. Al-Barakaty,¹ Sergey Prosandeev,^{2,*} Dawei Wang,³ B. Dkhil,⁴ and L. Bellaïche²

¹*Physics Department, Jamoum University College,
Umm Al-Qura University, Makkah, Saudi Arabia*

²*Physics Department and Institute for Nanoscience and Engineering,
University of Arkansas, Fayetteville, Arkansas 72701, USA*

³*Electronic Materials Research Laboratory,
Key Laboratory of the Ministry of Education and International Center for Dielectric Research,
Xi'an Jiaotong University, Xi'an 710049, China*

⁴*Laboratoire Structures, Propriétés et Modélisation des Solides,
CentraleSupélec, Université Paris-Saclay,
CNRS-UMR8580, Grande Voie des Vignes,
92295 Châtenay-Malabry Cedex, France*

Abstract

An atomistic numerical scheme is developed and used to study the prototype of relaxor ferroelectrics, that is $\text{PbMg}_{1/3}\text{Nb}_{2/3}\text{O}_3$ (PMN), at finite temperature. This scheme not only reproduces known complex macroscopic properties of PMN, but also provides a deep microscopic insight into this puzzling system. In particular, relaxor properties of PMN are found to originate from the competition between (1) random electric fields arising from the alloying of Mg and Nb ions belonging to different columns of the periodic Table within the same sublattice; (2) the simultaneous condensation of *several* off-center \mathbf{k} -points as a result of a specific short-range, antiferroelectric-like interaction between lead-centered dipoles; and (3) ferroelectric-like interactions. Such origins contrast with those recently proposed for the homovalent $\text{Ba}(\text{Zr,Ti})\text{O}_3$ solid solution, despite the fact that these two materials have similar macroscopic properties – which therefore leads to a new and comprehensive understanding of relaxor ferroelectrics.

Relaxor ferroelectrics have attracted much attention since their discoveries more than five decades ago. In particular, numerous studies have been conducted on the prototype of ferroelectric relaxors, that is lead magnesium niobate $\text{PbMg}_{1/3}\text{Nb}_{2/3}\text{O}_3$ (PMN), and have revealed anomalous features, which are also inherent to some magnetic systems^{1,2} therefore extending their significance beyond ferroelectrics. For instance, PMN adopts a dielectric response-*versus*-temperature function that possesses a rounded peak, having a large magnitude and is strongly dependent on the frequency of the applied *ac* electric field, while PMN remains *macroscopically* non-polar, down to the lowest temperatures^{3,4}. Measurements of its inverse dielectric permittivity⁵ as a function of temperature have also revealed an unusual deviation from linear behavior for a specific temperature, which is now known as the Burns temperature, T_B ⁶.

Several conflicting models have been proposed to understand the microscopic origin of relaxor ferroelectrics, in general, and of PMN, in particular. A popular belief to explain their macroscopic anomalies is the existence of the so-called polar nano-regions (PNRs)⁵⁻⁹. These polar correlations are thought to appear at T_B and to freeze on cooling, as similar to dipole glass state. Another widespread and alternative model is that PMN owes its unusual properties to the development of a state formed by nanoscale multidomains¹⁰⁻¹³. Indeed, Ref. [12] proposed that quenched random fields (arising from the fact that the randomly distributed Mg and Nb cations possess different nominal ionic charges) prevent the normal ferroelectric state to take place and rather break it down into a nanodomains state. Reference [10] suggested that the large magnitude of the dielectric permittivity of PMN is then due to the side-wall motion in these nanodomains. Actually, the glassy-state *versus* nanodomains model is still debated and no consensus or satisfactory description of the real structure currently exists. As detailed in some reviews^{3,13-15}, other concepts have also been considered to explain the peculiar properties of PMN, including chemically-ordered regions¹⁶ possessing large dielectric response^{17,18}, overbonded oxygen ions¹⁹, polaronic mechanism^{20,21}, and the coexistence of ferroelectric and antiferroelectric couplings²². It is also unclear if the recent mechanism that has been determined from first-principles-based calculations on the homovalent (Ba,Zr)TiO₃ relaxor ferroelectric – that is the coexistence within the same material of ferroelectrically active and ferroelectrically inactive (silent) ions²³ – holds for PMN.

A comprehensive understanding of lead-based relaxors, in general, and its representative compound, i.e. PMN, in particular, is therefore still lacking, despite the introduction of remarkable pioneering analytical approaches, such as the Random-Site²⁴, Spherical-Random-Bond-Random-Field²⁵, and Soft Pseudospin Glass²⁶ models as well as other models²⁷. One reason behind this

paucity of knowledge is that finite-temperature properties of heterovalent lead-based relaxors are rather challenging to mimic due, e.g., to the facts that its mixed B -sublattice is formed by ions that are chemically very different (Mg and Nb in PMN) and that the other cation sublattice possesses (lead) ions that strongly desire to move away from their ideal positions^{7,28,29}.

The goal of this paper is to report the development and results of a new atomistic numerical scheme that is able to realistically mimic the subtle and intriguing features of PMN, and which further provides a deep insight (that we believe to be unprecedented) into the microscopic description of this prototypical relaxor ferroelectric. In particular, this scheme reveals the major importance of random electric fields as well as complex and unexpected antiferroelectric-like interactions (involving *several* off-center vectors in the reciprocal space), allowing to understand the properties of PMN. The use of this scheme also resolves the aforementioned issues about the microscopic nature of PMN, and also elucidates the (controversial) effect of chemical ordering on properties of PMN.

As detailed in the Supplemental material^{30–35}, we developed an effective Hamiltonian (H_{eff}) for PMN. Its degree of freedom are (1) the local soft-mode in unit cell i , \mathbf{u}_i , which represents the collective motion of Pb, Mg/Nb and oxygen ions associated with the lowest transverse optical phonon branch³⁶. \mathbf{u}_i is therefore directly proportional to the local electric dipole moment in cell i . It is technically chosen to be centered on the Pb sites, as consistent with the known fact that lead ions significantly move off-center in Pb-based perovskites^{28,29,37–40}; (2) Nb/Mg-centered dimensionless local displacements, \mathbf{v}_i , that are related to the inhomogeneous strain inside each cell³⁶; and (3) the homogeneous strain tensor, η_H ³⁶. Such effective Hamiltonian also depends on $\{\sigma_j\}$ variables that characterize the atomic configuration of the PMN solid solution. More precisely, $\sigma_j=+1$ or -1 corresponds to the presence of a Mg or Nb atom located at the B-lattice site j , respectively⁴¹. Here, we average properties over 30 different alloy configurations, all randomly selected and frozen during the simulations, in order to mimic well disordered PMN systems⁴². Monte-Carlo simulations using this H_{eff} are performed using $18 \times 18 \times 18$ supercells (29,160 atoms) with periodic boundary conditions. Note that the parameters entering the expressions of the total energy of the H_{eff} of PMN are initially determined by conducting first-principles computations^{43–45} on small cells. However, these parameters are also allowed to vary from their first-principles values in the present work, in order to obtain a better agreement with experiments. In particular and as discussed below, we found that two types of these parameters play an important role on properties of PMN and need to be carefully adjusted from their computed values. They

are (i) the short-range parameter called j_5 in Ref.³⁶, that characterizes a specific interaction between second-nearest neighbors (e.g., between different Cartesian components of the local modes that are centered on two Pb sites that are the closest along the $\langle 110 \rangle$ pseudo-cubic directions); and (ii) the magnitude of the coefficients denoted by $Q_{|j-i|}(\sigma_j)$, which represent the strength and direction of the so-called random electric fields^{12,24,46,47}.

Figure 1a reports the dielectric susceptibility, χ , of disordered PMN as a function of temperature, computed from the cumulant method detailed in Ref.⁴⁸ and involving the local soft modes (χ therefore corresponds to the experimental situation for which *small* electric fields are applied). The dielectric susceptibility of PMN has a rounded peak while, as shown in the right inset of Fig. 1b, no polarization is numerically found to appear on zero field cooling, even at the lowest temperatures. Such features are consistent with experiments on PMN and are characteristics of relaxor ferroelectrics³⁻⁵. They also contrast with the case of “normal” ferroelectrics for which the dielectric susceptibility has a sharp peak around the paraelectric-to-ferroelectric phase transition temperature. Other information revealed by Fig. 1a is that χ follows a Curie-Weiss law⁴⁹ $C/(T - T_0)$ (where T is the temperature, and with $C = 1.27 \times 10^5 \text{K}$ and $T_0 = 400 \text{K}$) for temperatures above $\simeq 600 \text{K}$, while it deviates from this law for temperatures below 600K . Interestingly, this latter temperature corresponds to the Burns temperature ($T_B = 620 \text{K}$) reported for PMN⁶ below which there is a known deviation of χ from the Curie-Weiss law, and above which the Curie-Weiss law is well obeyed with $C = 1.25 \times 10^5 \text{K}$ and $T_0 = 396 \text{K}$ according to Ref.⁵ (note that similar values of the Curie-Weiss constant were obtained in other experiments, e.g., $C = 2.05 \times 10^5 \text{K}$ and $C \approx 10^5 \text{K}$ in Refs¹¹ and¹⁴, respectively). Comparisons between the predicted and measured values of both T_B and T_0 , as well as of the Curie-Weiss constant, therefore attest to the accuracy of the simulations after careful selection of the effective Hamiltonian parameters. It is also worth mentioning that χ exhibits rather large error bars for temperatures below T_B , in general, and close or below to its peak, in particular. This indicates that properties of PMN are rather sensitive to the atomic configuration. Moreover, T_0 , which usually corresponds to the Curie temperature in normal ferroelectrics, can be identified here as the so-called T^* temperature inherent to relaxors^{5,8,50-53}. We will come back to these points later on.

We also conducted simulations for which disordered PMN is cooled down under a *dc* electric field that is oriented along the pseudo-cubic [111] direction, and having Cartesian components equal to $1.0 \times 10^7 \text{V/m}$ along the x -, y -, and z -axes (the magnitude of this field is therefore $\sqrt{3} \times 10^7 \text{V/m}$). Under these circumstances, PMN adopts a significant electrical polarization along

the direction of the applied field below a certain temperature, and, correspondingly, a large *dc* susceptibility (not shown here), which differs from the susceptibility, obtained by the cumulant method, and that can be considered as one of the main features of the relaxors and glasses²⁶. Interestingly, such polarization remains finite when this field is removed at low temperature. The left inset of Fig 1b reveals that this polarized state (obtained at 10 K here) possesses some degrees of disorder in it since not all the dipoles are aligned along the [111] direction – which is in contrast with the case of a typical ferroelectric like BaTiO₃ but is consistent with what was observed experimentally in PMN by local probes such as the nuclear magnetic resonance technique in Ref. [7]. We numerically find that this degree of disorder originates from the random electric fields existing inside PMN. The system is then heated *under no electric field* starting from this low-temperature, polarized state. The resulting temperature dependence of the Cartesian components of the supercell average of the local mode, $\langle \mathbf{u} \rangle$, is displayed in Fig. 1b (note that the *x*-, *y*- and *z*-axes are chosen along the pseudo-cubic [100], [010] and [001] directions, respectively). One can, e.g., see that the *x*-, *y*- and *z*-Cartesian components of $\langle \mathbf{u} \rangle$ are all predicted to have a magnitude of 0.050 a.u at 10K, 0.045 a.u. at 150 K, and of 0.039 at 250K, which corresponds to a polarization of 0.54C/m², 0.49C/m², and 0.43C/m², respectively, that is oriented along [111]. These magnitudes agree rather well with measurements providing 0.46C/m² at temperature close to 0K⁵⁴ and 0.41C/m² at 150K⁵⁵ as well as with first-principles calculations yielding values ranging between 0.40C/m² and 0.65C/m² at 0K^{38,39} – which further emphasizes the capability of our H_{eff} to realistically mimic the complex properties of PMN. Figure 1b also indicates that the polarization decreases on heating and then, at about 250 ± 50 K, experiences a sudden jump down leading to its vanishing. Such striking behavior has indeed been experimentally reported, with the temperature associated with this jump being called the depolarization, temperature, T_{depol} , and being equal to $\simeq 210 - 230$ K for (111) crystals^{12,56-58}. The temperature at which this jump occurs is also linked to the freezing temperature, T_f , below which PMN is non-ergodic¹² – as evidenced in Fig. 1b by the different ground states obtained depending on the cooling regime (zero-field cooling or removing of electric field after field cooling).

Having demonstrated the predictive capability of our simulations at both global/macrosopic (cf Fig. 1a) and local/nanosopic (left inset of Fig. 1b) levels, let us now provide a microscopic insight of PMN by showing, in Figures 2 (a-d), snapshots of the dipolar patterns within a (*x*, *y*) plane for different temperatures, when the system is cooled under no field. These snapshots reveal that correlated clusters, usually referred to as polar nanoregions (PNRs) and inside which dipoles

are nearly parallel to each other and contain at least two Pb-centered dipoles, indeed exist in PMN, as suggested in Refs.^{6,40,58–61} and similar to the case of the homovalent BZT relaxor^{23,42,62,63}. These PNRs are delimited by red lines in Figs 2(a-d), and are numerically found by using the same Bayesian algorithm as in Refs.^{42,62} from instantaneous snapshots (configuration of the last Monte-Carlo sweep for any investigated temperature). Their average (dimensionless) size⁶⁴ is computed as $\langle s \rangle = \langle N^2 \rangle / \langle N \rangle$, where N is the number of Pb sites belonging to a PNR, and the brackets denote the average over all the PNRs existing inside the supercell. Figure 2e displays the predicted temperature dependency of $\langle s \rangle$. The data of Figs 2 indicate that $\langle s \rangle$ rapidly grows and the number of PNRs becomes larger upon cooling below T_B , in general, and below T_f , in particular (note that PNRs containing a single Pb dipole are included in the definition of $\langle s \rangle$, which explains why $\langle s \rangle$ is not equal to 0 above the Burns temperature). Indeed, Figs. 2c and 2d reveal the large number of PNRs below 200K, and Fig. 2e demonstrates an average cluster size of 19. Interestingly, such size corresponds, in one dimension, to a length of about 72Å, which is similar to the spatial correlation length of 62.4Å obtained experimentally by neutron diffuse scattering⁵⁸ at 10K. Note that the Supplemental Material also discusses the dynamic *versus* static characters of these PNRs for different temperatures (see Fig. 1 there), which is found to be in line with experimental findings^{51,58}. As a result, on decreasing temperature, the size (cf Figs. 2) and the degree of the static character (see the Supplemental Material³⁰) of the polar correlations in PMN are increasing to get a microscopic configuration, below T_f , which is described by many nanosize clusters that are separated from a few isolated, non-vanishing dipoles – which contrasts with the case of BZT²³.

Let us now discuss and reveal the key features at the origin of the aforementioned microscopic description and properties of PMN relaxor. For that, we, first, decided to compute correlations between dipoles as follows:

$$\theta_{\alpha,\alpha}(\mathbf{r}) = \frac{1}{N_{sc}} \sum_i \frac{u_{i,\alpha} u_{i+r,\alpha}}{|\mathbf{u}_i \cdot \mathbf{u}_{i+r}|}, \quad (1)$$

where the index i runs over all the N_{sc} Pb-sites of the supercell and where \mathbf{u}_i and \mathbf{u}_{i+r} are the local modes in cell i and in the cell centered on the Pb atom distant from \mathbf{r} from the cell i , respectively⁶⁵. $u_{i,\alpha}$ and $u_{i+r,\alpha}$ are the α -Cartesian component of \mathbf{u}_i and \mathbf{u}_{i+r} , respectively. Note that $\theta_{\alpha,\alpha}(\mathbf{r})$ is equal to 1/3 for any α (i.e., x , y or z) and for any \mathbf{r} in the hypothetical case for which the dipoles all have the same magnitude and are all lying along the pseudocubic [111] direction. Positive

and negative signs of $\theta_{\alpha,\alpha}(\mathbf{r})$ are representative of correlations and anticorrelations, respectively, between the α -component of \mathbf{u}_i and $\mathbf{u}_{i+\mathbf{r}}$. Figures 3a and 3b display $\theta_{x,x}(\mathbf{r})$ for the \mathbf{r} vectors lying in the (x, y) plane, at 10K and for two different realizations of disordered PMN. While these two correlations between the x -components of the local modes can present some differences in, e.g., shape, anisotropy and values at some particular \mathbf{r} distances, they also share a remarkable feature: the existence of significant *anticorrelations* in regions of space centered about $\mathbf{r}_1 = \pm 4.5a_{lat}\mathbf{x}$ and $\mathbf{r}_2 = \pm 4.5a_{lat}\mathbf{x} \pm 9a_{lat}\mathbf{y}$ in our $18 \times 18 \times 18$ supercell, where a_{lat} is the lattice constant of the 5-atom primitive cell and where \mathbf{x} and \mathbf{y} are unit vectors along the x - and y -axis, respectively. Note that we also numerically found (not shown here) (1) similar anticorrelations of the x -components of the local modes in the (x, z) plane for regions centered about \mathbf{r}_1 and $\mathbf{r}_3 = \pm 4.5a_{lat}\mathbf{x} \pm 9a_{lat}\mathbf{z}$ (where \mathbf{z} is the unit vector along the z -axis); and (2) similar anticorrelations of the y - and z -components of the local modes in the planes and around positions that can be deduced by cyclic permutations from the case of the anticorrelations between the x -components of the local modes. These anticorrelations can be thought as representative of antiferroelectric-like interactions existing inside PMN, which is consistent with the previously suggested idea that antiferroelectricity plays some role in relaxor behaviors^{22,23,66-69}. Moreover, such anticorrelations between the x -components of the local modes were further found to be associated with the Fourier transform of the distribution of the x -component of the local modes inside the supercell⁷⁰ being significant at *several off-center vectors* of the first Brillouin zone. Typically, in our $18 \times 18 \times 18$ supercells, these off-center \mathbf{k} -points are among the eight given by $\frac{2\pi}{9a_{lat}}(\pm\mathbf{x} \pm \mathbf{y})$ and $\frac{2\pi}{9a_{lat}}(\pm\mathbf{x} \pm \mathbf{z})$, and that will be denoted as $\mathbf{k}_{\max,i}$ in the following, where i runs from 1 to 8. Note that (1), for the case of the x -components of the local modes, these $\mathbf{k}_{\max,i}$ lie, close to Γ , along the $\Gamma - M$ lines of the first Brillouin zone, where the M points are given by $\frac{\pi}{a_{lat}}(\pm\mathbf{x} \pm \mathbf{y})$; (2) the $\mathbf{k}_{\max,i}$ are given by $\frac{2\pi}{9a_{lat}}(\pm\mathbf{x} \pm \mathbf{y})$ and $\frac{2\pi}{9a_{lat}}(\pm\mathbf{y} \pm \mathbf{z})$ for the Fourier transform of the y -components of the local modes, and by $\frac{2\pi}{9a_{lat}}(\pm\mathbf{x} \pm \mathbf{z})$ and $\frac{2\pi}{9a_{lat}}(\pm\mathbf{y} \pm \mathbf{z})$ for the Fourier transform of the z -components of the local modes; and (3) the $\mathbf{k}_{\max,i}$ vectors also depend on the size of the periodic supercell used in the simulations. For instance, they are still lying among the $\Gamma - M$ lines of the first Brillouin zone when using $N \times N \times N$ supercells with $N = 12, 14$ or 16 , but their magnitude is now equal to $\sqrt{2} \frac{2\pi}{Na_{lat}}$ in these cases (note that these \mathbf{k} -points are thus not located at zone *boundaries*). As a result, one can infer that the magnitude of the “real” $\mathbf{k}_{\max,i}$ for which the Fourier transforms of the Cartesian-components of the local modes are maximum ranges in-between 0.0884 and 0.1571 in $\frac{2\pi}{a_{lat}}$ units (note that this magnitude can also be rather sensitive to the j_5 parameter).

Furthermore, Figures 3c and 3d display the temperature evolution of the square of the Fourier transform of the x -component of the local dipoles configuration at some of these $\mathbf{k}_{max,i}$ points for the two alloy configurations associated with Figs 3a and 3b, respectively. Interestingly, these quantities are non-zero only below $450 \pm 50\text{K}$, which we identify as the so-called T^* critical temperature of relaxors and which we also considered to be equal to T_0 in the aforementioned Curie-Weiss relationship for the dielectric response. Note that different measurements provide values of 350K ⁵⁰, 400K ^{5,8,51}, and 500K ⁵² for T^* in PMN, and that both hyper-Raman⁷¹ and inelastic neutron⁷² scattering techniques pointed out to a condensation of the soft polar mode at respectively 400K and 340K . It is interesting to realize that the onset of anticorrelations shown in Figs. 3c and 3d occurs in a temperature range that is consistent with the condensation of the M - and R -point zone boundary soft modes observed in PMN by Swainson et al.⁶⁹ between 400K and 450K . Such experimental data (i) therefore cover a rather wide temperature interval inside which our prediction falls in and (ii) which can be understood by realizing that Figs. 3c and 3d reveal that this T^* can depend on the alloy configuration (and thus should be experimentally dependent on the sample preparation and the spatial (and probably time) scale resolution of the experimental technique). As a matter of fact, Fig. 3c gives a T^* close to 400K while Fig. 3d yields a value closer to 450K . Note that the Supplemental Material also provides additional details about the effect of atomic ordering on properties of PMN systems. Figures 3c and 3d further show that the square of the Fourier transform increases when decreasing the temperature below T^* until reaching a rather significant value that also strongly depends on the atomic configuration used to represent disordered PMN. For instance, the two configurations resulting in the correlations depicted in Figs. 3a and 3b possess values of about 12% for $\frac{2\pi}{9a_{lat}}(\mathbf{x} + \mathbf{z})$ and of about 7% for $\frac{2\pi}{9a_{lat}}(\mathbf{x} + \mathbf{y})$ of the total spectra gathering the Fourier transforms at all possible \mathbf{k} -points at 10K , respectively. Such results indicate that, as similar to the BZT case²³, anticorrelations begin to occur at the T^* critical temperature and strengthen as the temperature is reduced below T^* . The fact that Figs. 3c and 3d demonstrate that *several* of these symmetry-related $\mathbf{k}_{max,i}$ exist for any disordered atomic configuration at any temperature below T^* makes the disordered PMN different from an incommensurate crystal, for which only a *single* off-center \mathbf{k} -point condenses at a critical temperature in one macroscopic domain^{15,73}. The simultaneous condensation of several \mathbf{k} -points presently discovered here is also a key ingredient of the so-called weak crystallization theory⁷⁴ and is also likely consistent with the idea of phonon localization advanced in Refs. [75 and 76] to explain the relaxor behavior in PMN (note also that the occurrence of correlated regions localized in real space, such as the PNRs, also automatically

imply the existence of more than one k-point in the Fourier transform of the local modes). It is important to know that increasing the magnitude of a specific short-range order parameter between second nearest neighbors (namely, the j_5 coefficient indicated in the Method Section) was numerically found to enhance both the strengths of the anticorrelations and of the Fourier transform of the local modes at $\mathbf{k}_{\max,i}$ for any temperature below T^* , therefore demonstrating its relevance to understand PMN, as well as, the possibility for tuning relaxor-like properties.

Interestingly, we can also infer that, in addition to j_5 , the random electric fields are also key ingredients at the very heart of the properties of PMN. To illustrate this fact, we conducted additional simulations in which the random electric fields are switched off (practically, the $Q_{|j-i|}(\sigma_j)$ coefficients are imposed to be null). Figures 1c and 1d show the resulting temperature dependency of the dielectric response and of the x -component of the $\langle \mathbf{u} \rangle$ supercell average of the local modes (which is also equal to its y and z components), respectively, when the system is progressively cooled from high temperature down to 10K. Comparing Fig. 1a with Figs 1c and 1d tells us that the random electric fields play a primordial role in the relaxor behavior of PMN: without them, disordered PMN would display a first-order transition at around $550 \pm 50\text{K}$ (that is characterized by a large and sharp peak in the dielectric susceptibility) above which the system is macroscopically paraelectric while below which it is ferroelectric with an electrical polarization lying along the pseudo-cubic [111] direction and increasing in magnitude as the temperature is reduced (as shown by Fig. 1d). Figure 1c further shows that the Curie-Weiss law is also followed for temperatures above 750K with a corresponding T_0 of 633K, when random fields are not included in the simulations. Surprisingly, for temperatures ranging between $T = 550\text{K}$ to 750K (that is “just” above the transition temperature) another Curie-Weiss law is obeyed, one for which T_0 is now very close to 500K. We numerically find that the existence of these two different Curie-Weiss laws originates from the appearance of the aforementioned (j_5 -driven) AFE-like features for temperatures ranging between 550K to 750K. On the other hand, these AFE-like features are found to vanish in favor of a ferroelectric state for temperatures smaller than $550 \pm 50\text{K}$, that is below the phase transition – as demonstrated by the inset of Fig. 1d revealing that the low-temperature polar state is homogeneous, when random electric fields are turned off. Such findings therefore demonstrate the strong competition between ferroelectric and AFE-like interactions. Moreover, It is also important to know that the temperature at which the peak of the dielectric response occurs when random fields are neglected does *not* neither necessarily coincide with the Burns temperature nor T_0 or T^* of the true disordered PMN system (i.e., incorporating the $Q_{|j-i|}(\sigma_j)$ coefficients). As a matter

of fact, we numerically found that it is possible to find *different* combinations between the aforementioned j_5 and $Q_{|j-i|}(\sigma_j)$ parameters giving the same T_0 and T_B as in Fig. 1a for disordered PMN (in general the larger j_5 is in magnitude the bigger $Q_{|j-i|}(\sigma_j)$ is for these combinations), while the position of the peak of the dielectric response reported in Fig. 1c (in case of no random electric field) does depend on this combination. Note that, technically speaking, we also needed to vary a third effective Hamiltonian parameter, along with j_5 and $Q_{|j-i|}(\sigma_j)$ coefficients, to have a fixed T_0 temperature. This third parameter is the harmonic coefficient of the local electric dipoles, and is therefore directly related to the strength of the ferroelectric instability at the zone-center. Such facts (further) demonstrate that ferroelectric degrees of freedom, antiferroelectric-like motions and random fields all interact with each other to produce the striking properties of disordered PMN, and thus all need to be accounted for to understand this complex system, in particular, and lead-based relaxors, in general.

In summary, we use a new effective Hamiltonian method to study finite-temperature properties of PMN. This numerical technique reproduces known anomalous striking signatures of this prototype of relaxor ferroelectrics, therefore demonstrating its accuracy and capability. It also reveals the nanoscale picture of PMN and the microscopic origins of its properties. It is also worth realizing that a similar technique was recently used to investigate the lead-free and homovalent $\text{Ba}(\text{Zr,Ti})\text{O}_3$ system²³. Comparing that study²³ to the present one reveals that different relaxor ferroelectrics can exhibit similar macroscopic properties but their microscopic origins can be fundamentally different: in one case, the difference in polarizability between the ions belonging to the mixed sublattice (that is Ti and Zr in $\text{Ba}(\text{Zr,Ti})\text{O}_3$) was found to be essential to reproduce relaxor behavior via the formation of small embedded polar nanoregions. On the other hand, in case of PMN, the major players are the random electric fields arising from the mixed B -sublattice, the strong short-range interactions between lead-centered electrical dipoles and the competition between ferroelectric and antiferroelectric interactions, which result in a complex nanodomain structure exhibiting anticorrelations associated with several off-center k -points. We therefore hope that the present work results in a deeper and broader knowledge of the fascinating class of relaxor ferroelectrics, and can also be useful for the understanding of other inhomogeneous systems with remarkable properties like colossal magnetoresistance or high-temperature superconductivity where competing states in the presence of random fields are key ingredients too⁷⁸.

This work is financially supported by N00014-12-1-1034 (S.P. and L.B.) and NSF grant DMR-1066158 (D.W.). D.W. also acknowledges support from National Natural Science Foundation

of China (Grant No. 51390472) and National Basic Research Program of China (Grant No. 2015CB654903).

* sprossan@uark.edu

- ¹ T. Kimura *et al.*, Phys. Rev. Lett. **83**, 3940 (1999).
- ² V. V. Laguta *et al.*, New Journal of Physics **16** 113041 (2014), doi:10.1088/1367-2630/16/11/113041.
- ³ L. E. Cross, Ferroelectrics **151**, 305 (1994).
- ⁴ G. A. Smolensky *et al.*, *Ferroelectrics and Related Materials*, (Gordon and Breach, New York 1981).
- ⁵ D. Viehland *et al.*, J. Appl. Phys. **68**, 2916 (1990).
- ⁶ G. Burns and F. H. Dacol, Phys. Rev. B **28**, 2527 (1983).
- ⁷ R. Blinc, V. V. Laguta, and B. Zalar, Phys. Rev. Lett. **91** 247601 (2003).
- ⁸ B. Dkhil *et al.*, Phys. Rev. B **65**, 024104 (2001).
- ⁹ P. M. Gehring *et al.*, Phys. Rev. Lett. **87**, 277601 (2001).
- ¹⁰ A. K. Tagantsev, and A. E. Glazounov, Phys. Rev. B **57**, 18 (1998).
- ¹¹ D. Fu *et al.*, Phys. Rev. Lett. **103**, 207601 (2009).
- ¹² V. Westphal, W. Kleemann, and M. D. Glinchuk, Phys. Rev. Lett. **68**, 847 (1992).
- ¹³ J. Hlinka, Journal of Advanced Dielectrics. **2**, 1241006 (2012.)
- ¹⁴ A. A. Bokov and Z.-G. Ye, J. Mater. Sci. **41**, 31 (2006).
- ¹⁵ R. A. Cowley *et al.*, Advances in Physics **60**, 229 (2011).
- ¹⁶ P. K. Davies, M. A. Akbas, J. Phys. Chem. Solids **61**, 159 (2000).
- ¹⁷ P. Ganesh *et al.*, Phys. Rev. B **81**, 144102 (2010).
- ¹⁸ S. Tinte *et al.*, Phys. Rev. Lett. **97**, 137601 (2006).
- ¹⁹ I. Grinberg *et al.*, Phys. Rev. Lett. **99**, 267603 (2007).
- ²⁰ V. S. Vikhnin *et al.*, Ferroelectrics **285**, 291 (2003).
- ²¹ R. F. Mamin and R. Blinc, Physics of the Solid State **45**, 942 (2003).
- ²² V. M. Ishchuk, V. N. Baumer, and V. L. Sobolev, J. Phys.: Condens. Matter **17**, L177 (2005).
- ²³ A. R. Akbarzadeh *et al.*, Phys. Rev. Lett. **108**, 257601 (2012).
- ²⁴ B. E. Vugmeister, and M. D. Glinchuk, Rev. Mod. Phys. **62**, 993 (1990).
- ²⁵ R. Pirc and R. Blinc, Phys. Rev. B **60**, 13470 (1999).
- ²⁶ D. Sherrington, Phys. Rev. Lett. **111**, 227601 (2013); Phys. Rev. B **89**, 064105 (2014).

- ²⁷ G. G. Guzmán-Verri, P. B. Littlewood, and C. M. Varma, *Phys. Rev. B* **88**, 134106 (2013).
- ²⁸ I.-K. Jeong *et al.*, *Phys. Rev. Lett.* **94**, 147602 (2005).
- ²⁹ W. Dmowski *et al.*, *Phys. Rev. Lett.* **100**, 137602 (2008).
- ³⁰ The Supplemental Material gives detailed information about the effective Hamiltonian scheme used here, and also reports results related to the static *versus* dynamical character of the PNRs and the influence of chemical ordering on properties of $\text{PbMg}_{1/3}\text{Nb}_{2/3}\text{O}_3$ systems.
- ³¹ A. L. Roytburd, *Phase Transitions* **45**, 1 (1993).
- ³² R. Hemphill, L. Bellaiche, A. Garcia, and D. Vanderbilt, *Appl. Phys. Lett.* **77**, 3642 (2000).
- ³³ O. Bidault *et al.*, *J. Appl. Phys.* **90**, 4115 (2001); C. Perrin *et al.*, *J. Phys.: Condens. Matter* **13**, 10231 (2001).
- ³⁴ N. Setter and L. E. J. Cross, *Appl. Phys.* **51**, 4356 (1980).
- ³⁵ C. Malibert *et al.*, *J. Phys.: Condens. Matter* **9**, 7485 (1997) .
- ³⁶ W. Zhong, D. Vanderbilt, and K. M. Rabe, *Phys. Rev. B* **52**, 6301 (1995); *Phys. Rev. Lett.* **73**, 1861 (1994).
- ³⁷ S. Vakhrushev *et al.*, *J. Phys.: Condens. Matter* **6**, 4021 (1994).
- ³⁸ N. Choudhury *et al.*, *Phys. Rev. B* **71**, 125134 (2005).
- ³⁹ S. A. Prosandeev *et al.*, *Phys. Rev. B* **70**, 134110 (2004).
- ⁴⁰ A. Naberezhnov *et al.*, *Eur. Phys. J. B* **11**, 13 (1999).
- ⁴¹ L. Bellaiche, A. Garcia, and D. Vanderbilt, *Phys. Rev. Lett.* **84**, 5427 (2000); *Ferroelectrics* **266**, 41 (2002).
- ⁴² S. Prosandeev, D. Wang, and L. Bellaiche, *Phys. Rev. Lett.* **111**, 247602 (2013).
- ⁴³ L. Bellaiche and D. Vanderbilt, *Phys. Rev. B* **61**, 7877 (2000).
- ⁴⁴ P. Hohenberg and W. Kohn, *Phys. Rev.* **136**, B864 (1964); W. Kohn and L. J. Sham, *ibid.* **140**, A1133 (1965).
- ⁴⁵ D. Vanderbilt, *Phys. Rev. B* **41**, 7892(R) (1990).
- ⁴⁶ J. Iñiguez and L. Bellaiche, *Phys. Rev. B* **73**, 144109 (2006).
- ⁴⁷ B. E. Vugmeister and H. Rabitz, *Phys. Rev. B* **57**, 7581 (1998).
- ⁴⁸ K. M. Rabe and E. Cokayne, *First-Principles Calculations for Ferroelectrics: Fifth Williamsburg Workshop*, (R. E. Cohen, ed., AIP, Woodbury, New York, p. 61, 1998).
- ⁴⁹ F. Jona and G. Shirane, *Ferroelectric crystals*. (Dover Publications, INC., New York, 1993).
- ⁵⁰ O. Svitelskiy *et al.*, *Phys. Rev. B* **68**, 104107 (2003).

- ⁵¹ C. Stock *et al.*, Phys. Rev. B **81**, 144127 (2010).
- ⁵² B. Dkhil *et al.*, Phys. Rev. B **80**, 064103 (2009).
- ⁵³ S. Prosandeev *et al.*, J. Appl. Phys. **114**, 124103 (2013).
- ⁵⁴ Z.-G. Ye and H. Schmid, Ferroelectrics **145**, 83 (1993).
- ⁵⁵ R. Sommer, N. K. Yushin, and J. J. van der Klink, Phys. Rev. B **48**, 13230 (1993).
- ⁵⁶ E. V. Colla *et al.*, Ferroelectrics **184**, 209 (1996).
- ⁵⁷ R. Pirc, Z. Kutnjak, and N. Novak, J. Appl. Phys. **112**, 114122 (2012).
- ⁵⁸ G. Xu *et al.*, Phys. Rev. B **69**, 064112 (2004).
- ⁵⁹ S. B. Vakhrushev *et al.*, Ferroelectrics **90**, 173 (1989).
- ⁶⁰ K. Hirota *et al.*, Phys. Rev. B **65**, 104105 (2002).
- ⁶¹ S. Vakhrushev *et al.*, J. Phys. Chem. Solids **57**, 1517 (1996).
- ⁶² S. Prosandeev *et al.*, Phys. Rev. Lett. **110**, 207601 (2013).
- ⁶³ D. Wang *et al.*, Nature Communications, DOI: 10.1038/ncomms6100 (2014).
- ⁶⁴ D. Stauffer and A. Aharony, *Introduction to Percolation Theory* (Taylor & Francis, London, 1994).
- ⁶⁵ A. R. Akbarzadeh *et al.*, Phys. Rev. B **70**, 054103 (2004).
- ⁶⁶ N. Takesue *et al.*, Phys. Rev. Lett. **82**, 3709 (1999).
- ⁶⁷ W. Hu *et al.*, Phys. Rev. B **89**, 140103(R) (2014).
- ⁶⁸ A. Tkachuk and C. Chen, Cond.-mat. archive 0303105v1 (2003).
- ⁶⁹ I. P. Swainson, C. Stock, P. M. Gehring, Guangyong Xu, K. Hirota, Y. Qiu, H. Luo, X. Zhao, J.-F. Li, and D. Viehland, Phys. Rev. B **79**, 224301 (2009).
- ⁷⁰ A. M. George, J. Íñiguez, and L. Bellaiche, Phys. Rev. B **65**, 180301 (R) (2002).
- ⁷¹ A. Al-Zein *et al.*, Phys. Rev. Lett. **105**, 017601 (2010).
- ⁷² S. B. Vakhrushev and S. M. Shapiro, Phys. Rev. B **66**, 214101 (2002).
- ⁷³ R. Blinc and A. P. Levanyuk (Eds.). *Incommensurate Phases in Dielectrics*, vols. 1, 2. (North-Holland, Amsterdam, 1986).
- ⁷⁴ E. I. Kats, V. V. Lebedev, and A. R. Muratov, Physics Reports **228**, 1 (1993).
- ⁷⁵ A. Bussmann-Holder, J. Phys.: Condens. Matter **24**, 273202 (2012).
- ⁷⁶ M. E. Manley *et al.*, Nature Communications **5**, 3683 (2014).
- ⁷⁷ V. Bovtun *et al.*, J. Eur. Ceram. Society **21**, 1307 (2001).
- ⁷⁸ E. Dagotto, Science **309**, 257 (2005).

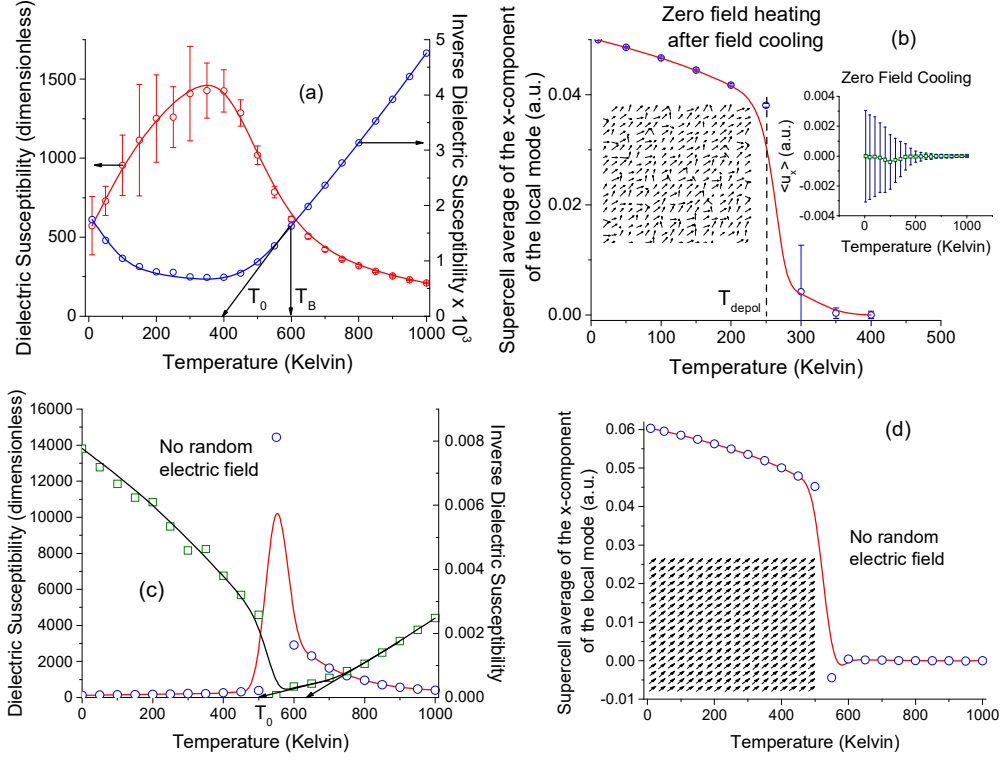


Figure 1. (color online) Predicted temperature dependence of several properties in PMN solid solutions. Panel (a) shows the dielectric susceptibility, and its inverse, when cooling down the disordered PMN system under no bias field. T_B and T_0 correspond to the Burns temperature and the critical temperature extrapolated from the Curie-Weiss law at high temperatures, respectively. Panel (b) displays the x -component of the supercell average of the local mode, $\langle \mathbf{u} \rangle$, (which is equal to its y - and z -components) when heating the system under no field, after having cooled it under an electric field and then having removed this field at 10K. The depolarizing temperature is $T_{depol} = 250 \pm 50$ K and is indicated by a vertical dashed line. The left inset of Panel (b) shows an example of the dipolar configuration when the field is removed at 10K. The right inset of Panel (b) shows the x -component of $\langle \mathbf{u} \rangle$, but when the system is cooled under no field. The error bars in Panels (a) and (b) are those arising from computing averages over 30 different chemical configurations. Panels (c) and (d) show the dielectric susceptibility (as well as its inverse) and the x -component of the supercell average of the local mode (which is identical to its y - and z -components), respectively, when random fields are switched off. The left inset of Panel (d) displays the resulting dipolar configuration at 10K, when random fields are turned off.

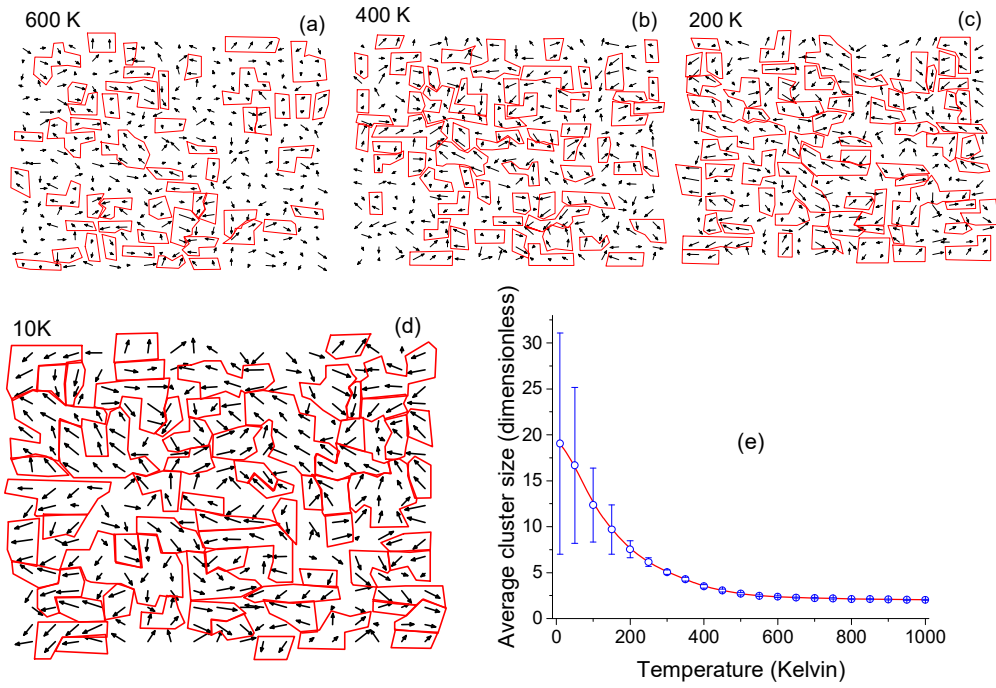


Figure 2. (Color online) Snapshots of the local modes' patterns within a (x, y) plane for different temperatures (Panels a-d) and temperature dependence of the average size of the polar nanoregion (Panel e), when disordered PMN is cooled under no field. In Panels (a-d), the corresponding temperature is indicated on the top left and the red lines delimit the PNRs. The error bars in Panel (e) are those resulting from incorporating 30 different chemical configurations into the computation of the averaged PNR size.

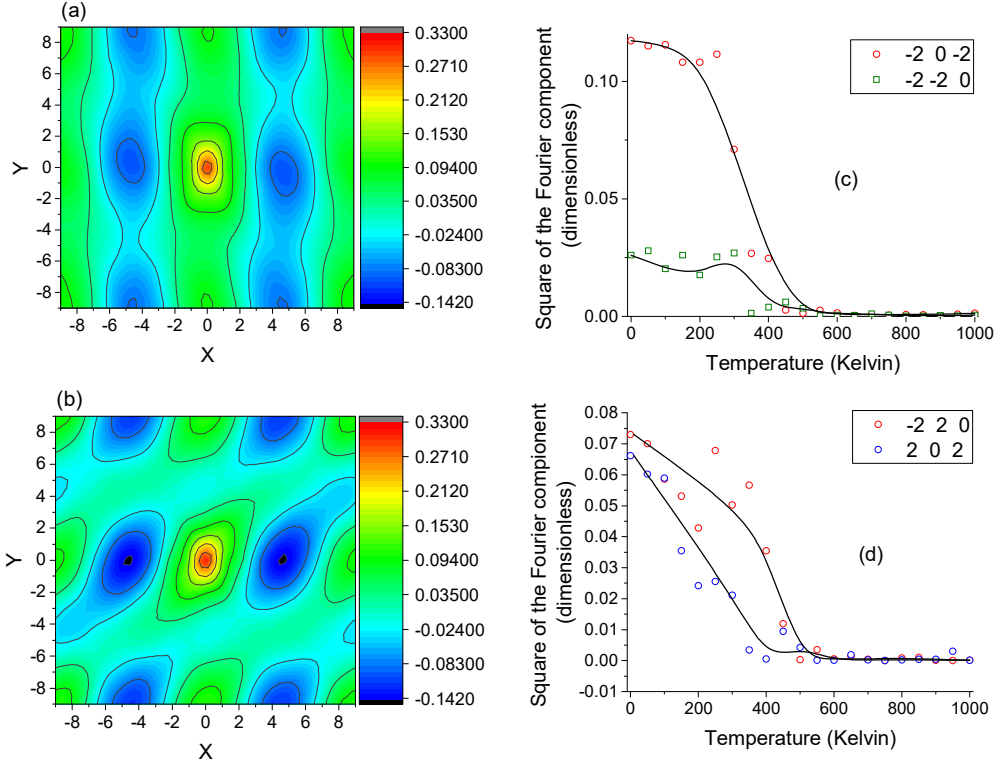


Figure 3. (Color online) Properties associated with anticorrelations and off-center points in disordered PMN. Panels (a) and (b) show the $\theta_{x,x}(\mathbf{r})$ correlation between the x -components of the local modes centered on lead atoms for the \mathbf{r} -vectors lying in the (x, y) plane at 10 K for two different realizations of the disordered PMN system. Panels (c) and (d) display the temperature dependence of the square of the Fourier transform of the x -component of the local modes' configurations for different $\mathbf{k}_{\max,i}$ points for the atomic configurations corresponding to Panels (a) and (b), respectively. The three integers, n_x , n_y and n_z indicated in the legends of Panels (c) and (d) index the $\mathbf{k}_{\max,i}$ points, that is such \mathbf{k} -points are given by $\frac{2\pi}{18a_{\text{lat}}}(n_x\mathbf{x} + n_y\mathbf{y} + n_z\mathbf{z})$ for our $18 \times 18 \times 18$ supercell. Note also that the square of the Fourier transform of the x -component of the local modes' configurations is invariant by inversion in the reciprocal space, i.e. $\frac{2\pi}{18a_{\text{lat}}}(n_x\mathbf{x} + n_y\mathbf{y} + n_z\mathbf{z})$ and $\frac{2\pi}{18a_{\text{lat}}}(-n_x\mathbf{x} - n_y\mathbf{y} - n_z\mathbf{z})$ have precisely the same value of the Fourier transform.